Role of intra-domain heterogeneity on ion and polymer dynamics in block polymer electrolytes: Investigating interfacial mobility and ion-specific dynamics and transport

Nicholas F. Pietra,<sup>a</sup> Andrew G. Korovich,<sup>a</sup> Priyanka M. Ketkar,<sup>b</sup> Thomas H. Epps, III,<sup>b,c,d</sup> and Louis A. Madsen<sup>a</sup>

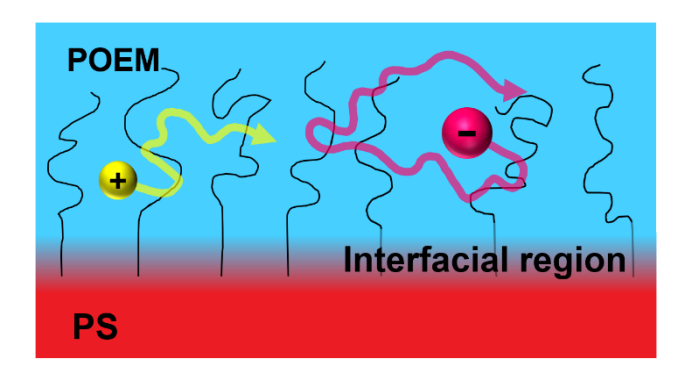
<sup>a</sup>Department of Chemistry and Macromolecules Innovation Institute, Virginia Polytechnic Institute and State University, Blacksburg, Virginia 24061, United States

<sup>b</sup>Department of Chemical & Biomolecular Engineering, University of Delaware, Newark, Delaware 19716, United States

<sup>c</sup>Department of Materials Science & Engineering, University of Delaware, Newark, Delaware 19716, United States

<sup>d</sup>Center for Research in Soft matter & Polymers (CRiSP), University of Delaware, Newark, Delaware 19716, United States

# For Table of Contents use only



### Abstract

Block polymers show promise as solid-state battery electrolytes due to the optimization of conductive and mechanical properties enabled via tuning of block chemistry and length. We investigate a polystyrene-block-poly(oligo-oxyethylene methacrylate) (PS-b-POEM) electrolyte doped with various lithium salts to investigate the role of molecular structure on ion transport properties and on local ion dynamics and associations. Anion charge becomes more delocalized with increasing size, reducing the coupling between salt ions while increasing coupling between ion and polymer chain motions and creating a more mobile overall environment. We observe support for this ion-polymer coupling via <sup>1</sup>H, <sup>7</sup>Li and <sup>19</sup>F NMR spectroscopy, from which we obtain ion-specific mobility transition temperatures that differ from the polymer glass transition temperature. We also note faster transport and weaker local energetic interactions with anion size using temperature-dependent NMR diffusometry. <sup>1</sup>H NMR spectroscopy further elucidates polymer chain dynamics and enables quantification of the temperature-dependent fraction of the conducting block that is immobile near the PS-POEM domain interface. NMR thus represents a species-specific and timescale-specific platform to quantify phase and interface behavior, and to correlate ion-specific transport with polymer chain dynamics.

### Introduction

Lithium-ion batteries, with their high energy density and long cyclability, have seen immense success in the energy storage field. However, solvents used for liquid electrolytes are flammable and offer no resistance to lithium dendrite formation, and as such present a serious risk of thermal runaway processes.<sup>1,2</sup> This factor has prompted research into solid-state (e.g., polymerbased) electrolytes, driven by the desire to remove flammable battery cell components as well as provide a single material acting as the mechanical/electrical separator and lithium ions (Li<sup>+</sup>) conductor. Poly(ethylene oxide) (PEO) doped with lithium salts has been a long-studied solid polymer electrolyte due to the polymer's low glass transition temperature  $(T_g)$  and the availability of coordinating (and ion-solvating) oxygens along the polymer chain.  $^{3-8}$  Above  $T_g$ , Li<sup>+</sup> can diffuse through PEO by changing coordination among the associating oxygens along the polymer chain, allowing the ions to move efficiently, but at the expense of the polymer's mechanical properties, leading to rapid battery failure. <sup>1,4,9,10</sup> This failure mechanism has led researchers to develop block polymer electrolytes with a rigid glassy phase for structural robustness combined with a mobile conducting phase, such as polystyrene-block-poly(oxyethylene oxide) (PS-b-PEO) electrolytes. 11-<sup>14</sup> In this work, we focus on polystyrene-block-poly(oligo-oxyethylene methacrylate) or PS-b-POEM (Figure 1a). Here, rather than PEO units forming the main chain, the POEM blocks have the ethylene oxide units grafted onto the polymer backbone as side chains, which improves conductivity near room temperature by limiting crystallization.<sup>15, 16</sup> In this study, we investigate the role of the anion molecular structure on the Li<sup>+</sup>, anion, and polymer dynamics within this system using NMR spectroscopy and diffusometry, and we present an approach to quantify the dynamically distinct regions at the interface between the hydrophilic and hydrophobic domains.

Additionally, we investigate the effect of different salt chemistries and concentrations on mobility temperature and its relationship to  $T_g$  values.

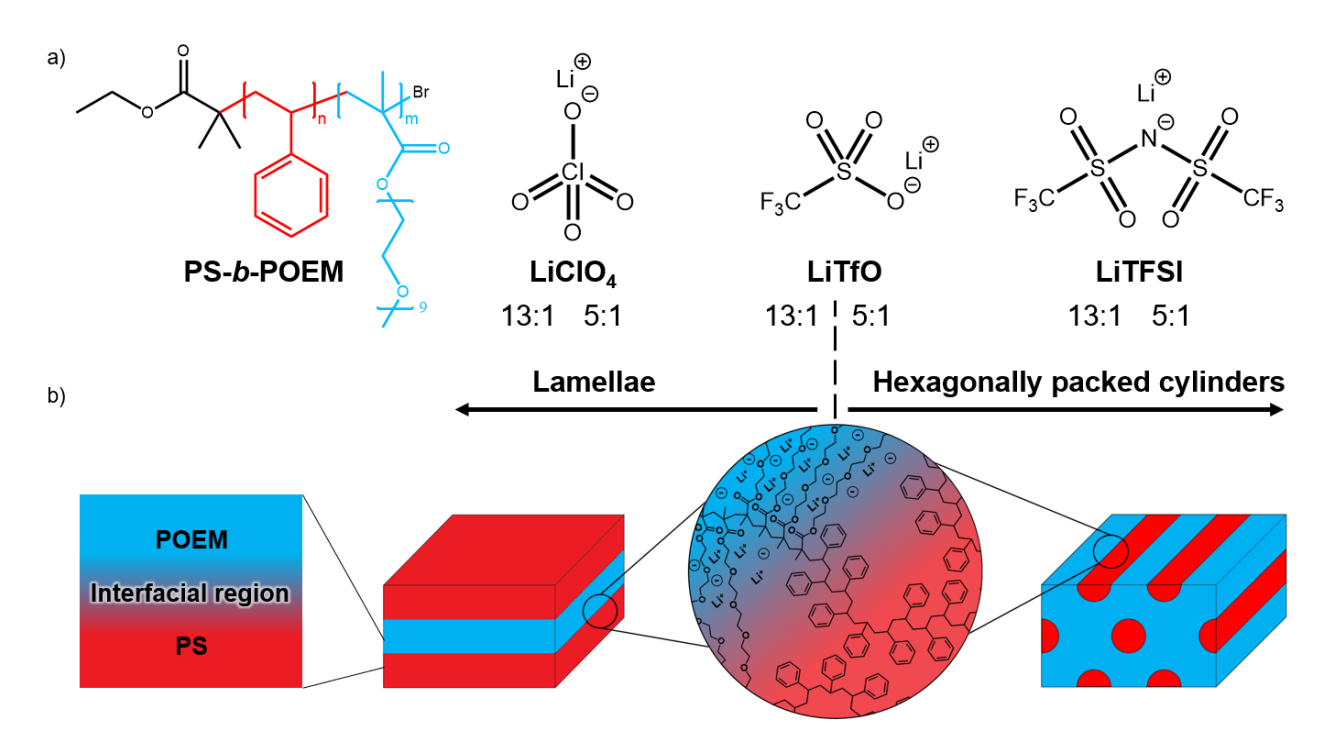


**Figure 1.** (a) Molecular structures of PS-*b*-POEM and lithium salts doped into this block polymer electrolyte: LiClO<sub>4</sub>, LiTfO, and LiTFSI. (b) Dependence of morphology on salt type and concentration. The 5:1 [EO]:[Li] LiTfO-doped and both LiTFSI-doped PS-*b*-POEM samples form a hexagonally packed cylindrical morphology with the PS phase occupying the cylindrical domains and the POEM forming the matrix. The 13:1 [EO]:[Li] LiTfO, both LiClO<sub>4</sub>-doped, and the neat PS-*b*-POEM form a lamellar morphology. SAXS results in support of these morphologies can be found in **Figure S10** and are discussed in detail in our companion paper.<sup>17</sup> Between the POEM and PS domains lies an interfacial region where the PS chains mix with the POEM chains, reducing the mobility of the normally fluid POEM chains and slowing ion motion.

To explore a range of anion chemistry and composition space, we doped the PS-b-POEM block polymer with LiTfO, LiTFSI, and LiClO<sub>4</sub> salts at ratios (ethylene oxide unit per lithium ion

or [EO]:[Li]) of 5:1 and 13:1. The morphology varies with salt type and concentration as shown in Figure 1b. We found a hexagonally packed cylindrical morphology (with PS as the cylinders and POEM as the matrix) for all LiTFSI-doped PS-b-POEM and 5:1 LiTfO-doped PS-b-POEM samples, and a lamellar morphology for the 13:1 LiTfO-doped PS-b-POEM sample and both 5:1 and 13:1 LiClO<sub>4</sub>-doped PS-b-POEM samples. The addition of salt enhances the segregation between polymer blocks, increasing the domain spacing with increasing salt concentration, and the specific ion-chain interactions cause the phase diagram to shift, altering the location of the morphological transition from lamellae to hexagonally packed cylinders with increasing anion size. 18-21 Both of these morphologies comprise a mobile (ion conducting) POEM phase and an immobile PS domain. However, at the interface between the two domains, the two polymer blocks mix, forming a gradient of each component across the interfacial region. In this region, the rigid PS chains reduce the mobility of the POEM chains, slowing ion motions. This change in polymer chain mobility between the domains (and including interfacial effects) results in a two-component <sup>1</sup>H NMR signal, with one component corresponding to mobile chains (POEM) and the other to immobile chains (PS plus immobilized POEM).

In NMR spectroscopy, when a nucleus moves faster along with molecular motions, magnetic spin interactions will fluctuate more rapidly. At a given molecular reorientation rate (and/or ion translation rate), the observed signal will be averaged over the orientations and environments experienced, leading to a given width of the observed line in the spectrum.<sup>22</sup> We use this principle to investigate both ion and polymer chain dynamics. As temperature and therefore the average kinetic energy of the system increases, nuclear spin motions transition from slow to fast, relative to the static coupling frequencies of spin-spin interactions (such as the magnetic dipole-dipole coupling) in the sample. Herein we designate such a transition temperature the

"mobility temperature," and we use NMR linewidths as a probe of the molecular tumbling and translational dynamics. Specifically, we use <sup>7</sup>Li and <sup>19</sup>F NMR spectroscopy to study ion dynamics and <sup>1</sup>H NMR spectroscopy for polymer chain dynamics.

To quantify and gain insights into ion-specific transport within the mobile fraction of the POEM phase, we employ pulsed-field-gradient (PFG) NMR diffusometry. NMR diffusometry represents a family of techniques for measuring the self-diffusion coefficients of multiple species in a sample (separated by their chemical shift and/or isotopic identities), and over a controlled range of time/length scales. Additionally, while most other types of diffusion measurements typically require a nonequilibrium system that must be initialized individually for each measurement (such as a prepared concentration gradient), NMR diffusometry can operate at equilibrium and at a fixed temperature. Herein, we probe <sup>7</sup>Li and <sup>19</sup>F nuclei, allowing us to measure separate cation and anion ion transport. Furthermore, by measuring diffusion coefficients as a function of temperature we can determine the activation energy of diffusion of these ions, which provides insight into the local energetics of ion transport. <sup>23-27</sup> Overall, in this study we quantify interfacial phase behavior and correlate ion-specific transport with polymer chain dynamics in PS-b-POEM.

# **Experimental**

## Materials

All materials were stored in a moisture-free, argon-filled glove box after purification. PS (number-average molecular weight  $[M_n] = 21.1 \text{ kg mol}^{-1}$ , dispersity [D] = 1.18), POEM ( $M_n = 24.1 \text{ kg mol}^{-1}$ , D = 1.08, each repeat unit contains 9 EO units on the side chain), and PS-*b*-POEM ( $M_n = 41.9 \text{ kg mol}^{-1}$ , D = 1.25, volume fraction of POEM [ $f_{POEM}$ ] = 0.46) were synthesized and purified as described in prior literature.<sup>28, 29</sup> Lithium bis(trifluoromethanesulfonyl)imide (LiTFSI, 99%,

Acros Organics), lithium trifluoromethanesulfonate (LiTfO, 99.995%, Sigma-Aldrich), and lithium perchlorate (LiClO<sub>4</sub>, 99+%, Acros Organics) were dried under constant vacuum at 150 °C for 48 h. Anhydrous tetrahydrofuran (THF, >99%, Optima, not stabilized, Fisher-Scientific) was obtained from a Pure Process Technology, LLC solvent system, in which THF from an argonfilled keg was passed through two packed alumina columns.

# Electrolyte preparation

The polymers (PS-b-POEM and POEM) and salts (LiTFSI, LiTfO, and LiClO<sub>4</sub>) separately were dissolved in anhydrous THF at ~20 wt% and stirred for at least 3 h, all in an argon-filled glove box. The appropriate masses of polymer and salt stock solutions were then mixed to achieve the desired salt concentrations relative to neat polymer, [EO]:[Li<sup>+</sup>] = 13:1 and [EO]:[Li<sup>+</sup>] = 5:1, in which [EO] and [Li<sup>+</sup>] are the molar concentrations of EO units and Li<sup>+</sup>, respectively. These salt and polymer solutions were stirred for at least 3 h, then dried under constant vacuum for 16 h at 25 °C and then for 10 h at 120 °C. The dried electrolytes were stored in an argon-filled glove box prior to characterization.

# NMR spectroscopy and diffusometry

All NMR experiments were performed as static-sample, solid-state ("wideline") experiments. The PS-b-POEM block polymer (BP) samples were quickly packed into the bottom of a 5 mm NMR sample tube in ambient atmosphere. The packed samples were dried by immersion in a sand bath at 120 °C and under constant vacuum for 48 h to ensure that any moisture introduced outside the glove box would be removed. To prevent oxidative degradation of the polymer, the dried samples were flame sealed while still under vacuum, wrapped in aluminum foil to reduce light exposure, and stored in a refrigerator prior to characterization via NMR. The POEM homopolymer (HP) samples were viscous fluids that adhered to the walls of the sample tube. To

cleanly pack the HP samples, the specimens were first packed into a  $3 \times 2 \times 10$  mm (outer diameter  $\times$  inner diameter  $\times$  length) glass tube. The homopolymer-loaded tube was inserted into a 5 mm NMR sample tube before drying and sealing in an identical manner to the BP samples.

The NMR spectra and diffusion data were obtained using a Bruker Avance III 400 MHz/9.4 T widebore spectrometer equipped with a high gradient diffusion probe (Bruker Diff50) paired with a 5 mm <sup>7</sup>Li/<sup>31</sup>P radiofrequency (RF) coil insert for <sup>7</sup>Li measurements, and a 5 mm <sup>1</sup>H RF coil insert for <sup>1</sup>H and <sup>19</sup>F measurements. All NMR experiments were measured across a temperature range of -40 to 80 °C with ≥ 5 min of thermal equilibration before acquiring data.

The 1D NMR spectra were acquired at each temperature using 16 scans with a 90° pulse length of 4.5  $\mu$ s for  $^{1}$ H, 5.5  $\mu$ s for  $^{19}$ F, and 6.25  $\mu$ s for  $^{7}$ Li. The acquisition times for these experiments ranged from 0.003 - 0.04 s for  $^{1}$ H, 0.004 - 0.35 s for  $^{19}$ F, and 0.005 - 0.04 s for  $^{7}$ Li NMR depending on the sample and temperature, adjusted to maximize signal-to-noise ratio (SNR). Relaxation delay (D1) values were 1.5 s for proton, 2 s for lithium and 1 s for fluorine. The longitudinal relaxation time ( $T_1$ ) range for  $T_1$ H is 1 - 5 s, for  $T_2$ Li is 1 - 2 s, and for  $T_3$ F was 0.5 - 1 s.

Self-diffusion coefficients of the Li<sup>+</sup> cations and the fluorine-containing anions were obtained using the pulse-gradient stimulated echo (PGSTE) experiment on <sup>7</sup>Li and <sup>19</sup>F nuclei across the -40 to 80 °C temperature range.<sup>30, 31</sup> The Stejskal-Tanner equation (Equation 1) was used to fit the measured signal amplitude (*I*) as a function of the gradient strength (*g*).

$$I = I_0 \exp\left(-D\gamma^2 g^2 \delta^2 \left(\Delta - \frac{\delta}{3}\right)\right) \tag{1}$$

In Equation 1,  $I_0$  is the signal amplitude at g = 0,  $\gamma$  is the gyromagnetic ratio of the measured nucleus,  $\delta$  is the effective (rectangular) gradient pulse duration,  $\Delta$  is the diffusion time between gradient pulses, and D is the self-diffusion coefficient. These measurements used a 90° pulse time

of 5.5  $\mu$ s for <sup>19</sup>F and 6.25  $\mu$ s for <sup>7</sup>Li. The diffusion experiments used a repetition time of 2 - 4 s,  $\delta$  = 2 - 6 ms,  $\Delta$  = 50 - 500 ms, with a max gradient strength ranging from 720 - 2900 G/cm and the same acquisition times used for the 1D spectroscopy experiments (adjusting the length of the free induction decay at a given measurement temperature). The value of the diffusion encoding parameters (g, d, and D) within these ranges depends upon the specific sample and temperature of the experiment and were selected to achieve  $\geq$  85% signal attenuation in 16 gradient steps.

### **Results and Discussion**

Mobility temperature measurement via static solid-state <sup>7</sup>Li, <sup>19</sup>F, and <sup>1</sup>H NMR Spectroscopy

To investigate the temperature dependence of the ion mobility within the system, we obtained <sup>7</sup>Li and <sup>19</sup>F spectra over the -40 to 80°C temperature range. The relative mobility of the nuclei, or the rate at which the nuclei are moving between different magnetic environments, is reflected in the spectral linewidths. As the mobility of a nucleus increases, the linewidth (full width at half maximum, FWHM) of the observed peak decreases, as shown in Figure 2 and Figure 3. The <sup>19</sup>F nucleus has a nuclear spin  $I = \frac{1}{2}$ , and therefore, the FWHM can be measured directly from the spectra. However, the  $^{7}$ Li nucleus is quadrupolar (nuclear spin I = 3/2), which causes it to have two components: a narrow component comprised of a central transition, which is present in all <sup>7</sup>Li nuclei regardless of magnetic environment, and a broad component comprised (in this case) of a superposition of "satellite" transitions that arises from a random distribution of locally anisotropic magnetic environments (see Section S1). To properly measure the linewidth of this multicomponent spectrum, we deconvoluted the spectrum by fitting it using a linear combination of a broad (Gaussian) and a narrow (Lorentzian) function (Figure S1). A Lorentzian function was used to describe the central transition<sup>22</sup> and a Gaussian function was used to describe the superposition of satellite peaks, as is typical of such random distributions. Plotting the FWHM of the  ${}^{7}\text{Li}$  and  ${}^{19}\text{F}$  spectra against temperature T results in the trends seen in **Figure 2** and **Figure 3**, which we fit using an empirical arctangent function (Equation 2).<sup>29</sup>

$$FWHM = K \tan^{-1} \left( \frac{T - T_{mobility}}{T_{final} - T_{mobility}} \right) + C$$
 (2)

K is an overall width parameter, C is a shift value equal to the average between the largest and smallest measured FWHM,  $T_{mobility}$  in this article represents the temperature at the midpoint of the transition (where the  $2^{nd}$  derivative of this function is zero), and  $T_{final}$  is the temperature at the endpoint (plateau width value) of the transition. Because this inflection point reflects the onset temperature at which the nuclei become mobile, we will refer to this  $T_{mobility}$  as the "mobility temperature." We then compare  $T_{mobility}$  values to the  $T_g$  values measured via DSC, which are measured as being the midpoint of the transition in heat capacity. The minor difference in the definition of  $T_{mobility}$  here as compared to a previous study is discussed in detail in Section S2.<sup>29</sup>

Figure 2 shows the linewidth vs. temperature plots for the PS-*b*-POEM block polymers (BP). In addition to measuring the <sup>7</sup>Li and <sup>19</sup>F linewidths (to quantify *T<sub>mobility</sub>* for each ion), we also measured the polymer chain mobility temperature from the <sup>1</sup>H spectral linewidths (Figure 4c and Figure 5c). While the observed <sup>7</sup>Li and <sup>19</sup>F spectra only contain signals from single molecular species/environments, the <sup>1</sup>H NMR spectra contain signals from both the PS and POEM blocks, each of which have the potential to show a broad *and* narrow component corresponding to immobile and mobile chains, respectively. To fit these spectra in a similar manner to those obtained via <sup>7</sup>Li and <sup>19</sup>F NMR spectroscopy, we first investigated the temperature dependence of the NMR linewidth for the neat PS homopolymer (HP) (Figure S4) and found that over the temperature range of interest (-40 to 80 °C) the measured width of the PS peak (34 kHz) did not change. This value was then used as a constraint for the broad component width in the two-component fitting

process, and this process was applied to the PS-*b*-POEM <sup>1</sup>H NMR spectra. At lower temperatures the POEM peak becomes obscured by the broad PS signal, preventing a reliable fit to extract this linewidth component.

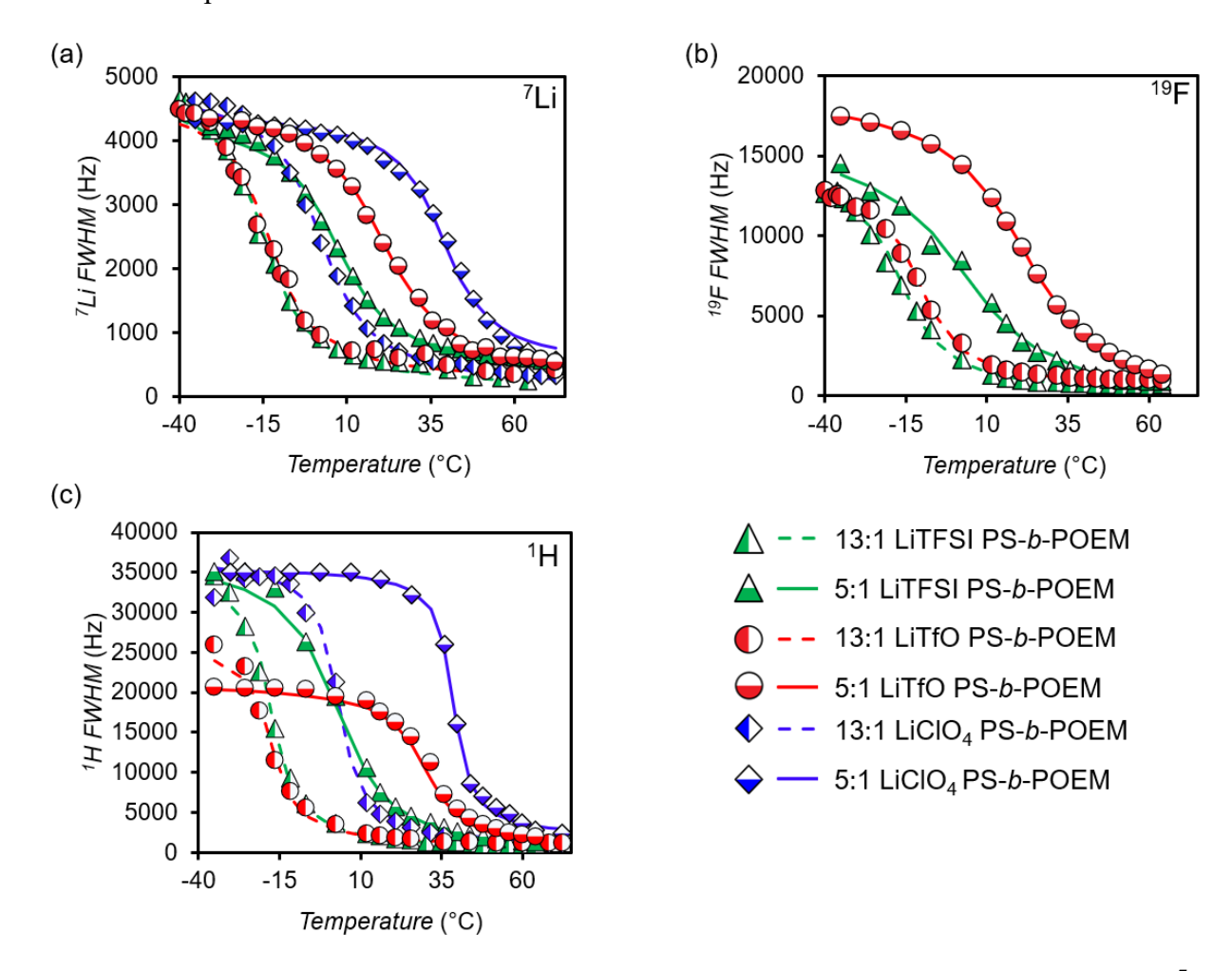


**Figure 2.** Temperature dependence of linewidth (FWHM) for PS-*b*-POEM electrolytes for (a)  $^{7}$ Li nuclei (Li<sup>+</sup>), (b)  $^{19}$ F nuclei (anions), and (c)  $^{1}$ H nuclei (polymer chains). Data points are the linewidth values from NMR spectroscopy measurements, and curves are fit to the data using Equation 2 to extract the mobility temperatures. Uncertainty in FWHM values is  $\pm 5\%$ . For each sample composition,  $T_{mobility}$  values for the cations and anions lie within a few degrees of each other, demonstrating consistency of this mobility temperature between nuclei and ionic species.

We also measured  $T_{mobility}$  for the POEM HP (**Figure 3**) to investigate any differences in dynamics due to confinement within the POEM domain, POEM chain stretching, and/or segmental mixing in the PS-b-POEM. **Table 1** compares the  $T_{mobility}$  values of the BP and HP, the differences between which are within 5 °C. This agreement between the mobility temperatures strongly indicates that the local dynamic environment the ions experience within the block polymer is on average very similar to that in bulk POEM, and implies that the immobilized POEM in the interfacial region has minimal effect on ion dynamics of the BP systems. The similarity of the mobility temperatures of the ions ( $^7$ Li and  $^{19}$ F) and of the POEM polymer chains ( $^1$ H) further supports the assertion that the ions are experiencing a similar local dynamic environment.

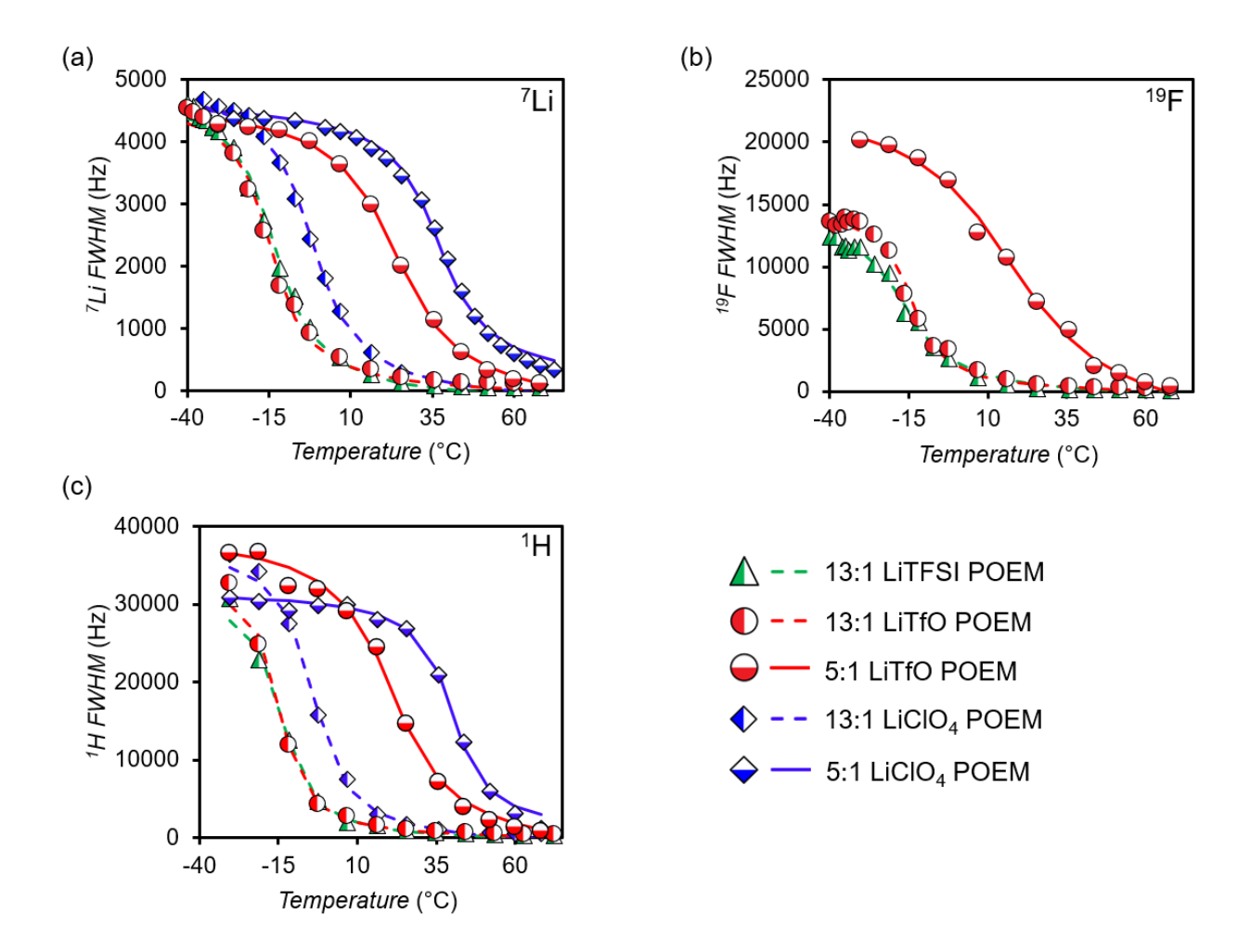


**Figure 3.** Temperature dependence of linewidth (FWHM) for POEM HP electrolytes for (a)  $^{7}$ Li nuclei (Li<sup>+</sup>), (b)  $^{19}$ F nuclei (anions), and (c)  $^{1}$ H nuclei (polymer chains). Data points are from NMR spectroscopy, and curves are fit to the data using Equation 2. Uncertainty in FWHM values is  $\pm 5\%$ . The  $T_{mobility}$  from the POEM HP is within a few degrees of the  $T_{mobility}$  observed in the PS-b-POEM BP, indicating the local dynamic environment probed by NMR linewidth is relatively insensitive to confinement (BP domain-dependent) effects.

**Table 1.** Mobility transition temperatures ( $T_{mobility}$ ) for PS-b-POEM (BP) and POEM (HP) electrolytes. Errors in  $T_{mobility}$  values are approximately +/- 5 °C.

	Midpoint	$T_g$ (DSC, °C)		
	<sup>7</sup> Li (cation)	<sup>19</sup> F (anion)	<sup>1</sup> H (polymer)	$(no \ salt = -65.4)$
PS-b-POEM BP				
13:1 LiTFSI	-14.5	-16.2	-17.5	-41.8
5:1 LiTFSI	6.8	0.3	2.6	-22.1
13:1 LiTfO	-13.1	-10.6	-17.3	-41.8
5:1 LiTfO	20.6	21.2	30.0	-13.4
13:1 LiClO <sub>4</sub>	2.2	N/A	3.0	-31.1
5:1 LiClO <sub>4</sub>	38.8	N/A	38.9	-10.2
POEM HP				
13:1 LiTFSI	-13.4	-16.8	-13.8	-41.8
13:1 LiTfO	-14.5	-14.2	-14.4	-41.8
5:1 LiTfO	23.9	16.9	21.0	-22.1
13:1 LiClO <sub>4</sub>	-1.8	N/A	-3.9	-31.1
5:1 LiClO <sub>4</sub>	36.8	N/A	40.1	-10.2

Comparison of the cation and anion  $T_{mobility}$  values to the glass transition temperatures of the conducting POEM phase from DSC (**Table 1**) shows that  $T_{mobility} > T_g$  by 26 to 49 °C depending on the anion chemistry and salt loading. This offset is most prominently seen in the 5:1 [EO]:[Li] samples due to their higher salt concentration. These specimens show  $T_{mobility} > T_g$  by 26 °C for the LiTFSI-doped samples, 34 °C for the LiTfO-doped sample and 49 °C for the LiClO4-doped samples. In these comparisons, we take the average of the cation and anion  $T_{mobility}$  values to compare with the POEM  $T_g$ . This trend indicates that the more diffuse the anion charge, the smaller the difference between  $T_{mobility}$  and  $T_g$ . We propose that this is due to the larger anions associating less strongly with the Li<sup>+</sup> cations, allowing the salt ions to associate more with the polymer chain instead of associating with each other (and thus reducing the influence of the salt ions on the conducting phase dynamics). This trend is validated by simulations reported by Shen and Hall, who investigated the role of ion size disparities on ion transport and concluded that larger anions reduce ion aggregation and improve ion conduction.<sup>32</sup> We also see a significant change in the  $T_g$  of the salt-doped samples when compared to the neat polymer. This change is likely due to the

ion-polymer associations slowing the polymer chain dynamics, causing the  $T_g$  to increase. The difference in  $T_g$  between the salt types and concentrations is most likely due to the differences in degree of ion dissociation, which impacts the transient cross-linking dynamics.<sup>32-34</sup> Additionally, these differences in association strengths of the salts can also help explain the differences in morphology we see across the different samples (**Figure 1**), because the stronger cation-anion associations will decrease the ion-polymer association strength. Thus, we see a lamellar structure in the LiClO<sub>4</sub> samples, but as the anion size increases, the ion-polymer association strength increases and the volume of the POEM phase increases to accommodate the larger ion pairs, thus transitioning the morphology into hexagonally packed cylinders (**Figure 4**).<sup>18-20, 32</sup>

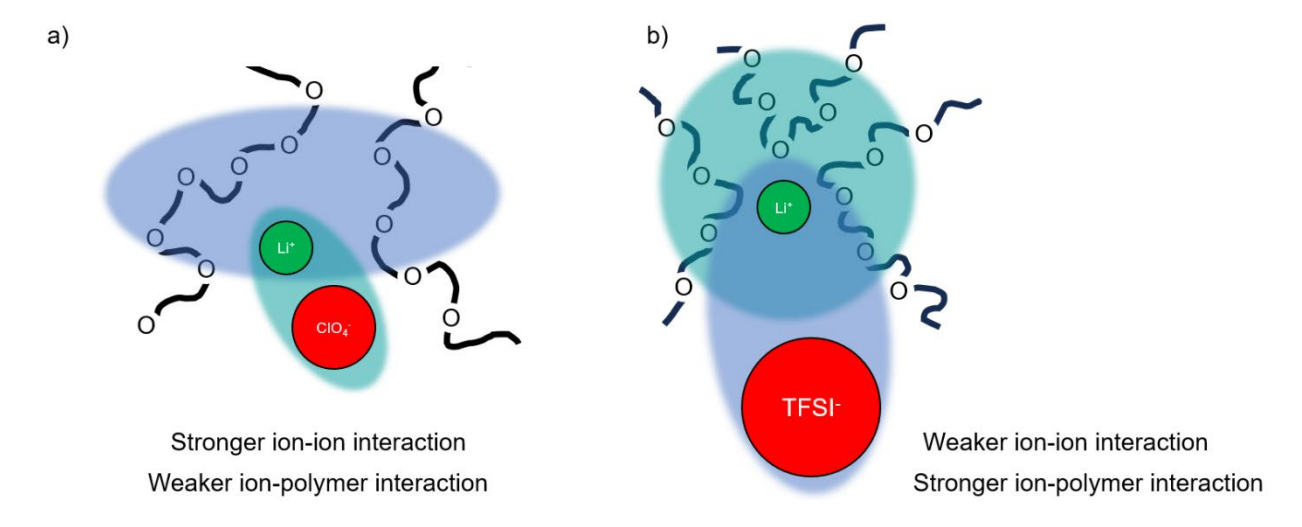


**Figure 4.** As the anion size increases, the association strength between the ions weakens, which allows the  $Li^+$  to interact more with the polymer chain.  $T_{mobility}$  of the ions conveniently probes this change in ionic interactions, as  $T_{mobility}$  shifts closer to the  $T_g$  of the conducting phase and causes the salt-bearing domain to swell and transition the polymer morphology from lamellar to hexagonally packed cylinders (POEM phase dominant).

Although **Figure 4** shows the role of anion size on the cation-polymer interaction, the similarity in  $T_{mobility}$  between the cation and anion suggests that they are experiencing a similar average dynamical (and thus spin-magnetic) environment. This observation is in line with the overall ion transport mechanism, in which lithium ions hop among ether oxygen atoms during segmental motion of the polymer chain while counter-anions strongly associate with and hop with the lithium ion aggregates. <sup>1, 4, 33, 35</sup> Although the ion-ion association strength decreases with an increase in anion size due to the decreased charge density, the cation-anion interactions are still strong enough that the ions experience a similar dynamical environment. The transport of both ions through the conducting POEM phase improves with increasing mobility of the polymer chain, and the temperatures at which the polymer chain mobilizes enough to transport these ions occurs at the  $T_{mobility}$  values reported in **Table 1**.

In short, these multinuclear ( ${}^{7}$ Li and  ${}^{19}$ F) NMR experiments allow us to independently study the mobility of both ions, from which we observe the degrees of their associations with the polymer chain by comparing  $T_{mobility}$  to  $T_g$ . Softer, larger anions enable (1) more close coupling of the cation and anion dynamics to the polymer chain dynamics by decoupling the salt ions from each other ( $T_{mobility}$  moves closer to  $T_g$ ), and (2) a more mobile overall environment at a given temperature (reduction of both  $T_{mobility}$  and  $T_g$ ).

# Polymer chain mobility and interfacial composition from <sup>1</sup>H NMR

We can further utilize our static-sample solid-state ("wideline") <sup>1</sup>H NMR experiments to probe polymer chain dynamics by partitioning the spectra into different components. These spectra have relatively broad linewidths for each peak (versus solution NMR spectroscopy), but we can use the two distinct components to unravel polymer phase behavior. In the <sup>1</sup>H spectrum, all peaks corresponding to the protons in the polymer chain overlap (see Figure 5). This spectrum can be deconvoluted into two components—a narrow component and a broad component. These two components of the <sup>1</sup>H spectrum report on the mobility of the protons in the polymer chain, with the broad component representing the total immobile chain portion of the block polymer. The relative intensities of these two components thus tell us the fraction of the bulk polymer that is immobile (f<sub>broad.H</sub>), which gives insight into the interfacial composition. Between the mobile POEM phase and immobile PS phase, there is an interfacial region (sometimes called an interphase), where the PS restricts the mobility of the POEM chains, resulting in less mobile POEM that cannot effectively conduct ions. As such, by measuring the amount of immobile POEM via our NMR spectra, we can determine the fraction of the total POEM within this interfacial region ( $f_{immobile,POEM}$ ). We have done this by deconvoluting the temperature-dependent  $^1\mathrm{H}$ spectra as described in Figure S6, then comparing the areas of the narrow component and broad

component to the expected stoichiometric fractions for POEM ( $f_{stoichiometric,POEM}$ ) and PS ( $f_{stoichiometric,PS}$ ). Thus, using Equation 3, we can quantify how much of the POEM block contributes to the broad component, from which, we obtain the fraction of immobile POEM.

$$f_{immobile,POEM} = \frac{f_{broad,H} - f_{stoichiometric,PS}}{f_{stoichiometric,POEM}}$$
(3)

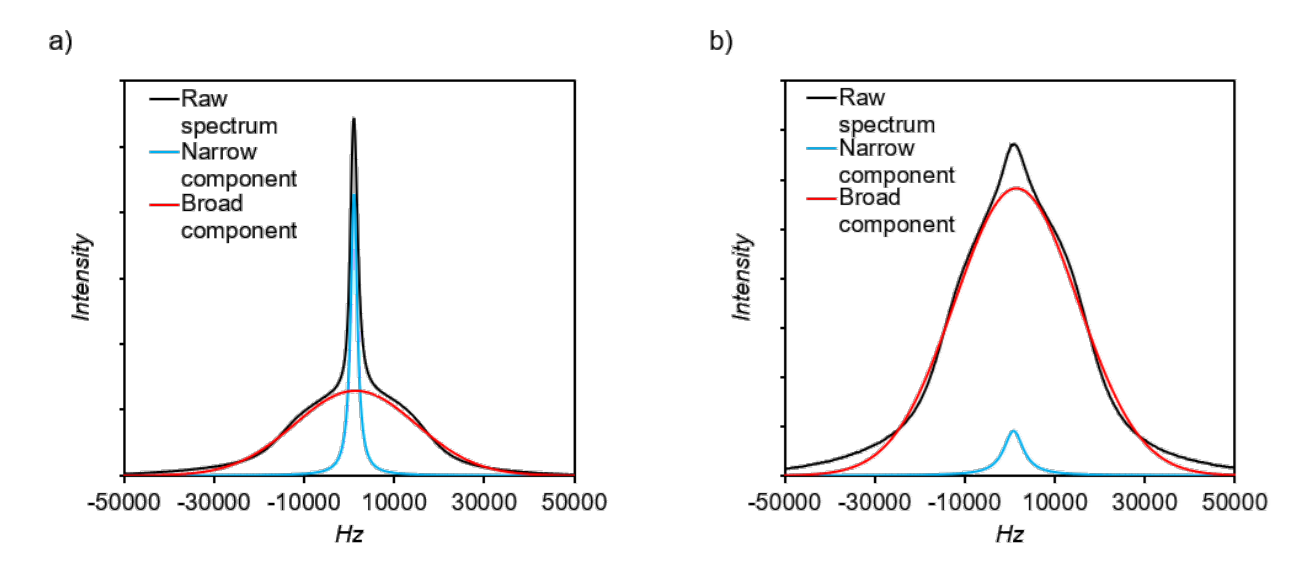


**Figure 5.** Representative static-sample, solid-state <sup>1</sup>H NMR spectra for PS-*b*-POEM doped with LiTfO at a ratio of [EO]:[Li] = 5:1 taken at 70 °C (a) and 25 °C (b). The raw spectrum contains two components, a narrow component (blue) and a broad component (red). The width of these components reports on the rotational mobility of the <sup>1</sup>H-containing polymer segments that contribute to these signals. The narrow component contains the proton signal from mobile parts of the POEM chains, and the broad component contains the proton signal from immobile POEM and PS chains. Although two-component fitting can reliably deconvolute the spectra at high temperature (a), as temperature decreases the POEM chains decrease in mobility, resulting in broad and narrow peak components that are closer in linewidth (b), thus decreasing the reliability of the fit.

In addition to this dynamics-based interfacial measurement from NMR spectroscopy, we can compare this fraction of immobile POEM in this interfacial region to the values obtained from small angle X-ray scattering (SAXS) and differential scanning calorimetry (DSC).<sup>36, 37</sup> The details of these measurements are found in Section S5 and are discussed in our companion paper.<sup>17</sup> **Figure 6** shows the agreement between these three different techniques.

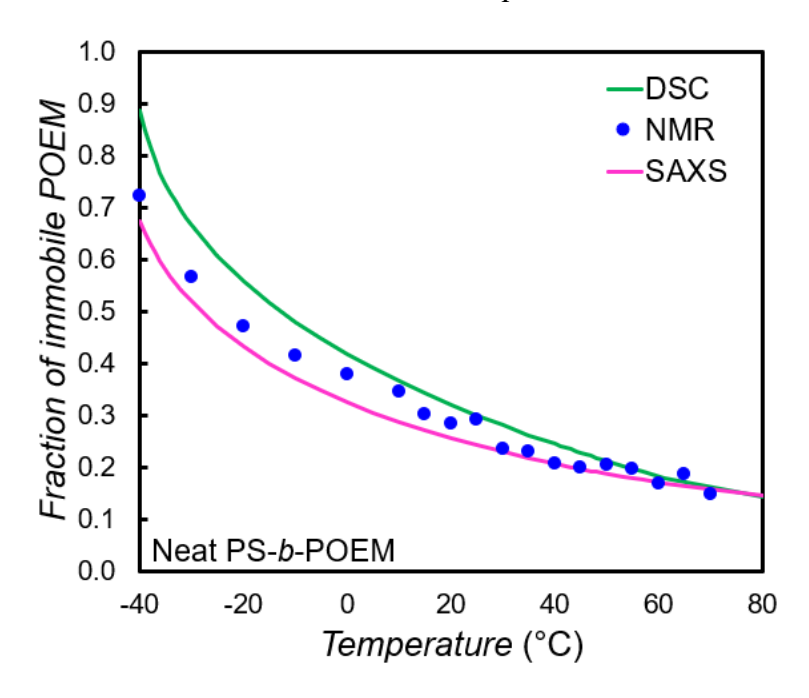


**Figure 6.** Immobile fraction of the conducting domain (POEM) versus temperature in neat (no lithium salt) PS-*b*-POEM using the purely dynamics-based NMR approach (blue), a predominantly structure-based SAXS approach (pink) adapted from literature<sup>37</sup> and a DSC approach (green) adapted from literature.<sup>36</sup> More detail on the SAXS and DSC approaches can be found in a our companion paper.<sup>17</sup>

All approaches to determining the fraction of immobile POEM agree well at higher temperatures, yielding the fraction of POEM within the interface of 15-20%. As temperature decreases, the NMR and DSC approaches deviate somewhat from the values given by the SAXS approach. This deviation is likely due to the SAXS approach measuring the compositional mixing

of the two phases while the DSC and NMR approaches measure the dynamics and chain relaxations of the system. As such, as temperature decreases, the fraction of total immobile POEM (including POEM that is not in the interface) increases, leading to a steeper increase in the fraction of immobile POEM reported by the NMR and DSC methods. Further discussion of this NMR approach for investigating the interface between the polymer phases can be found in our companion paper.<sup>17</sup>

The NMR method, based on integration of spectral components with different chain dynamics, is complementary to the DSC and SAXS approaches, and it can be more versatile. The SAXS method uses the widths of the SAXS profiles (which have different electron-density contrast) to measure the composition across the interface, but it is only applicable to lamellar morphologies and requires a rather complex model to extract the immobile fraction. Because the NMR method probes the polymer chain *mobility* via the transverse spin relaxation (signal decay) time, it is not restricted by morphological symmetry and can be used in non-lamellar systems such as the hexagonally packed cylinder system shown in Figure S9. Also, the NMR method requires no model other than the assumption of two distinct spectral components with different mobility and a simple least-squares fit to the two components. Note that the Gaussian nature of the broad fit component in this system should account for any distribution of chain mobilities across the interface, and the fits were very good without involving a distribution of line components. The DSC method, in contrast, observes the chain dynamics via the change in heat capacities between the homopolymer of the conducting phase and the PS-b-POEM block polymer. However, whereas DSC measures heat capacity changes detected by scanning temperature over the glass transition, NMR can measure the immobile fraction at any single fixed temperature, as an equilibrium measurement. Additionally, the interfacial measurement from DSC requires knowledge of the

volume fraction of the conducting domain obtained either by SAXS or by an estimation using molecular weight (Equation S6).<sup>36</sup> This requirement is unnecessary for the NMR approach, which only needs the stoichiometric ratio of the two blocks to directly compare with the integration ratio of the two components in the <sup>1</sup>H spectrum.

# Ion transport phenomena via NMR diffusometry

Using  ${}^{7}$ Li and  ${}^{19}$ F NMR diffusometry, we can also uncover aspects of cation and anion translational motions and how these motions couple to BP morphology and dynamics. We measured the diffusivity of both ions in the PS-*b*-POEM (BP) and in the POEM homopolymer (HP). **Figure 7** shows ionic diffusion coefficients for [EO]:[Li<sup>+</sup>] = 13:1 samples for both BP and HP. Unfortunately, due to equipment constraints combined with the short transverse relaxation times ( $T_2$ ) of the  $T_3$ Li and  $T_4$ P nuclei, we cannot access the diffusion of ions in [EO]:[Li<sup>+</sup>] = 5:1 samples. Additionally, due to fast  $T_4$ P and  $T_4$ P nuclei, we cannot access the diffusion, we cannot measure the anion diffusion for LiClO4-doped samples.

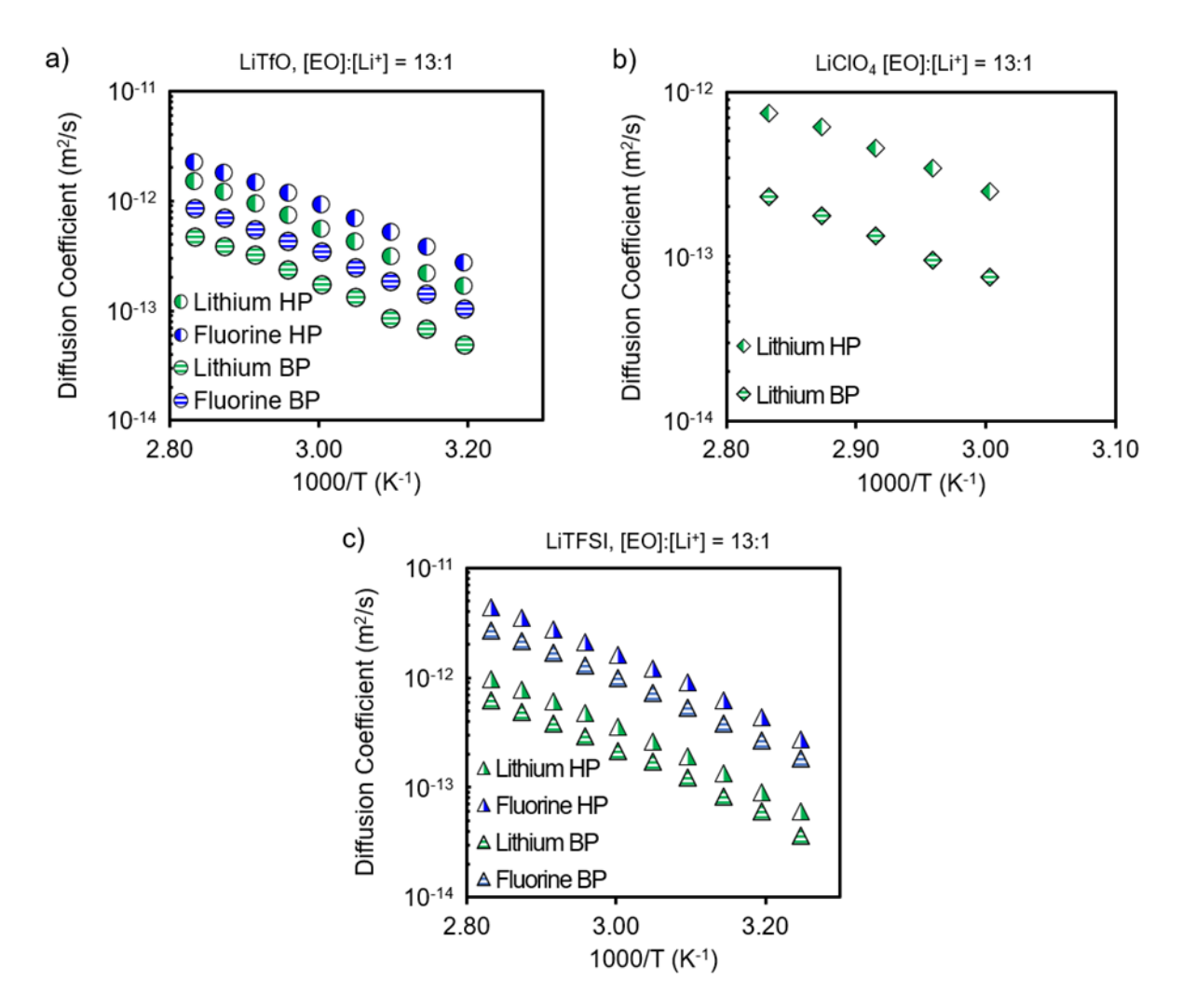


Figure 7. Temperature dependence of Li<sup>+</sup> cation ( $D_{\text{Li}^+}$ ) and fluorine-containing anion diffusion coefficients ( $D_{\text{TFSI-}}$  and  $D_{\text{TfO-}}$ ) in salt-doped PS-b-POEM BP and POEM HP. The LiTfO-containing sample (a) shows both cation and anions within the BP diffusing at 1/3 the rate of the HP instead of the 2/3 expected for the HP for a randomly oriented lamellar system such as this. <sup>10,38</sup> This trend also holds for the lamellar LiClO<sub>4</sub>-doped samples (b). The LiTFSI containing sample (c) shows the ion diffusion coefficients within the BP as 1/2 the value of the ions within the HP. This difference suggests a tortuosity factor  $\mathcal{T}$  (see below) of 2, which is above that expected from the simple geometric obstruction of the morphology. The uncertainty in ion diffusion coefficients is  $\pm 10\%$ .

Figure 7 shows diffusion coefficients of the anions and Li<sup>+</sup> in both the BP and HP samples, which give insights into what factors govern ion transport within the BP electrolyte. The anions clearly diffuse faster than the cations. Because the anions are larger than Li<sup>+</sup>, they have a lower charge density, which weakens their coordination. The weakened coordination reduces ion aggregation and causes the Li<sup>+</sup> to associate more with the oxygen atoms along the POEM chain, thus accelerating overall ion transport. The order of diffusion coefficients supports this assertion, as the ions in LiTFSI-doped samples are diffusing faster than those in the LiTfO-doped samples, and the LiClO4-doped samples diffuse the slowest.

Comparing the ion diffusion coefficients within the HP to those within the BP, we find that the BP samples containing LiTfO and LiClO<sub>4</sub> exhibit diffusion coefficients 1/3 as fast as their HP counterparts. The ion diffusion coefficients in the LiTFSI-doped BP are 1/2 as fast as the diffusion coefficients in the HP counterpart. As shown in **Figure 1**, the morphology of these salt-doped BP samples with [EO]:[Li<sup>+</sup>] = 13:1 are lamellar for the LiTfO- and LiClO<sub>4</sub>-doped samples and hexagonally packed cylinders for the LiTFSI-doped sample. The geometric factor for randomly oriented lamellae is  $f_{morphology} = 2/3$ , and the geometric factor for a randomly oriented hexagonally packed cylinder structure, with the conducting phase as the matrix is  $f_{morphology} = 1$ .<sup>10, 38, 39</sup> These geometric factors reduce average diffusion relative to a perfectly aligned phase and originate from how many of the three-dimensional axes (x, y, and z-axis) allow for diffusion to occur in a given morphology.<sup>39</sup> As such, these geometric factors assume an ideal system and neglect the effects of grain boundaries,<sup>25, 40</sup> molecular- or nanometer-scale defects,<sup>41-43</sup> or nanoconfinement of the rigid lamellae or rod walls<sup>26, 44</sup> or of the immobilizing interfacial region described previously, all of which could further restrict ion diffusion. Our lab has measured such effects in the past via

complementary NMR diffusometry techniques, and have described such effects using a tortuosity  $\mathcal{T}$  parameter:  $^{26, \, 40-45}$ 

$$\mathcal{T} = \frac{D_{local}}{D_{\infty}} \tag{7}$$

 $D_{local}$  represents "local" diffusion at a nanometer scale and  $D_{\infty}$  represents bulk diffusion measured at a diffusion time long enough to allow moving species to sample all heterogeneities in the sample. A  $\mathcal{T}$  value of 1 represents an ideal system, e.g., perfect domain connectivity and/or minimal grain defects or confinement effects. 41-43, 45 Our current BP samples have well-defined morphologies, and as such we can divide out the geometric factor ( $f_{morphology}$ ) from this tortuosity expression. Furthermore, we can represent  $D_{local}$  (for each ion) as the ion diffusion coefficient for our HP POEM ( $D_{lon,HP}$ ). This representation of  $D_{local}$  well approximates the average ion diffusion within the POEM domain of the BP since the thickness of our conducting POEM domain in the lamellar BPs is 13 to 23 nm, much larger than the scale of local molecular-scale motional processes.  $^{26, 41-43}$   $D_{\infty}$  can be represented using each ion diffusion coefficient for the BP samples ( $D_{lon,BP}$ ) at long diffusion time (D). The resulting decrease from  $D_{local}$  to  $D_{\infty}$  (or  $D_{lon,HP}$  to  $D_{lon,BP}$ ) then becomes:

$$D_{ion,BP} = \frac{f_{morphology}}{T} D_{ion,HP}$$
 (8)

 $f_{morphology}$  is the aforementioned geometric factor ( $f_{morphology}$ ), and  $\mathcal{T}$  is the tortuosity factor, which includes only the effects of hydrophilic domain wall effects, BP grain boundaries, and/or other morphological defects restricting the intra-domain diffusion of the ions within the BPs. We observe a value of  $\mathcal{T}\approx 2$  across both lamellar BP samples and a value of  $\mathcal{T}\approx 1.6$  for the LiTFSI-doped sample with a hexagonally packed cylindrical morphology (**Table S3**). These  $\mathcal{T}$  values indicate significant but not severe restrictions to transport from defects and confinement. The

decrease in tortuosity between the morphologies is likely due to the grain boundaries of the lamellar morphology hindering the ion transport more than the hexagonally packed cylinder morphology, the latter of which is inherently interconnected with any distribution of grain orientations. The idea that  $T \neq 1$  has precedent for BPs in investigations into diffusion of ions in BP morphologies with bicontinous phases (e.g., gyroid).<sup>46</sup> We do not need to explicitly consider the ion *obstruction effects of the polymer chain backbone* on the cation or anion diffusion as this occurs identically in the HP and BP.

We also probe the temperature dependence of D, which yields the activation energy ( $E_a$ ) of diffusion and can provide additional insights about local interactions occurring on the molecular ( $\sim 1$  nm or smaller) length scale, also called the ballistic or inertial length scale. Our group has developed a framework for understanding  $E_a$  in various systems with liquid-like diffusion.<sup>23-27, 41-45</sup> We find  $E_a$  of each ion in our samples using the Arrhenius equation:

$$D = D_0 e^{-\frac{E_a}{RT}} \tag{9}$$

D is the self-diffusion coefficient,  $D_0$  is the diffusion at infinite T or the "barrierless diffusion," and R is the gas constant.  $E_a$  for a given mobile species in our polymer samples describes the average energy of local intermolecular interactions that is involved in that species (ion) moving on the  $\sim 1$  nm scale, driven by the random collisions and local fluctuations.  $D_0$  can give additional insight into the local configurational degrees of freedom available for a given mobile species to diffuse. Table 2 shows the results of this Arrhenius analysis, which are generally comparable to reported values for PS-b-PEO systems.  $^{11, 12, 47}$ 

**Table 2.** Activation energies of cation and anion diffusion and  $D_{\theta}$  in PS-b-POEM and POEM electrolytes. Errors in  $E_{\theta}$  are approximately +/- 1.5 kJ/mol.

PS-b-POEM BP	Lithium $E_a$ (kJ/mol)	Lithium $D_{\theta}$ (m <sup>2</sup> /s)	Fluorine $E_a$ (kJ/mol)	Fluorine $D_{\theta}$ (m <sup>2</sup> /s)
LiTfO	53.6	4.28 x 10 <sup>-5</sup>	48.9	1.52 x 10 <sup>-5</sup>
LiTFSI	55.5	1.07 x 10 <sup>-4</sup>	55.1	$4.13 \times 10^{-4}$
LiClO <sub>4</sub>	54.9	$1.03 \times 10^{-4}$	N/A	N/A
POEM HP				
LiTfO	55.3	$2.49 \times 10^{-4}$	48.3	$3.29 \times 10^{-5}$
LiTFSI	56.5	$2.43 \times 10^{-4}$	57.2	$1.44 \times 10^{-3}$
LiClO <sub>4</sub>	55.8	$4.20 \times 10^{-5}$	N/A	N/A

We observe  $E_a$  values for  $\text{Li}^+$  of  $55 \pm 1.5$  kJ/mol, and furthermore that  $E_a$  values for TfO anion are 6 to 9 kJ/mol smaller than those for the TFSI anion and for the  $\text{Li}^+$ . The local energetics (enthalpics) of the TfO anion appear to promote faster  $\sim 1$  nm motion for this smaller anion. Additionally, comparing  $E_a$  of the ions in the BP to the HP samples, we see both ions have slightly lower  $E_a$  values in the BP samples across all samples. The small difference in  $E_a$  may imply an organization of the POEM phase in the BP system that improves local ion transport. For example, the constraining PS domain in the BP may create enhanced free volume near the interface between the PS phase and the POEM phase, 44 leading to lower  $E_a$  values.

Although the Li<sup>+</sup> measurements have  $D_0$  values within error of each other (a factor of 2-5), the fluorinated anions show a  $D_0$  that is a factor of ~ 100 larger for TFSI<sup>-</sup> than for TfO<sup>-</sup>. This difference in  $D_0$  might suggest that TFSI<sup>-</sup> has significantly more configurational freedom due to the more complex intramolecular anion configurations possible, along with a larger number of possible local arrangements of EO segments and Li<sup>+</sup> around this anion. While TfO<sup>-</sup> has somewhat lower  $E_a$ , its  $D_0$  is clearly smaller, suggesting fewer configurational degrees of freedom relative to TFSI<sup>-</sup>. Further studies will be required with a wider array of compositions and temperatures, to understand deeper aspects of local transport in these systems.

Conductivity from NMR Diffusometry and Haven ratio analysis

We can also use diffusion coefficients to predict the ionic conductivity using the Nernst-Einstein equation (Equation 10).<sup>23, 40, 48, 49</sup>

$$\sigma_{NMR} = \left(\frac{e^2}{kT}\right) \left(\frac{N}{V}\right) (D_+ + D_-) \tag{10}$$

where  $D_+$  and  $D_-$  are the diffusion coefficients of the cation and anion, respectively, and  $\left(\frac{N}{V}\right)$  is the number density of ions within the electrolyte. Because we could not collect D for the chlorine nuclei, we cannot determine  $\sigma_{NMR}$  for the LiClO<sub>4</sub> samples. **Figure 8** shows the conductivity values from the NMR diffusometry data for the 13:1 LiTfO- and LiTFSI-doped PS-b-POEM electrolytes ( $\sigma_{NMR}$ ) along with those obtained from impedance spectroscopy ( $\sigma_{IS}$ ).

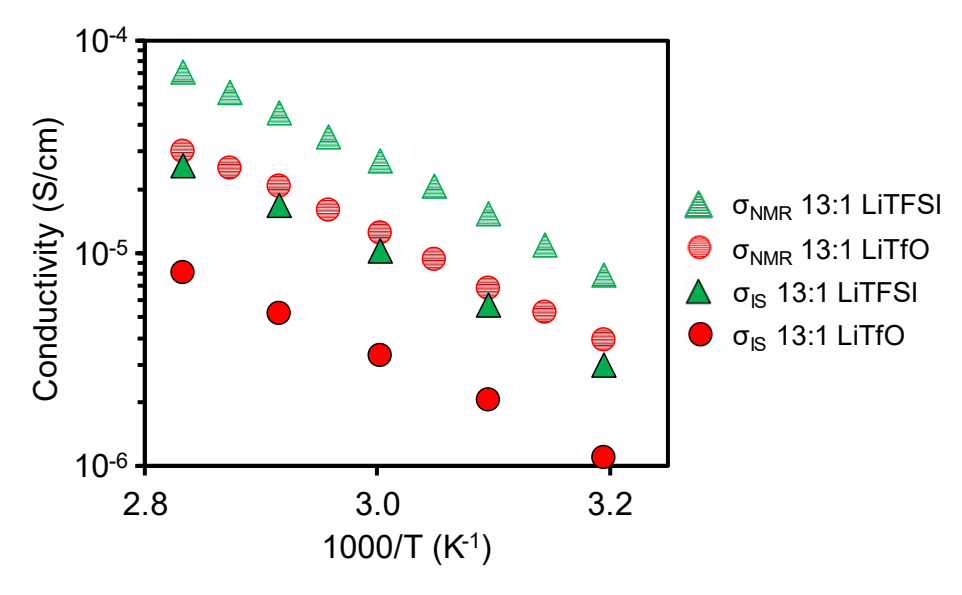


**Figure 8.** Temperature dependence of ionic conductivity within PS-b-POEM predicted from NMR diffusometry using the Nernst-Einstein equation ( $\sigma_{NMR}$ ) and that measured via impedance spectroscopy ( $\sigma_{IS}$ ). We could not measure D for the chlorine-containing anions, and thus only the LiTfO- and LiTFSI-doped samples were used to predict conductivity. Dividing  $\sigma_{NMR}$  by  $\sigma_{IS}$  gives Haven ratios of 2.7 for the LiTFSI-doped sample, and 3.6 for the LiTfO-doped sample. The uncertainty in  $\sigma_{NMR}$  is 14% and the uncertainty for the Haven ratio is 17%.

The conductivity values, regardless of approach, show the LiTFSI-doped samples with a higher conductivity than the LiTfO-doped samples. This trend makes sense, because the morphology of LiTFSI-doped samples is hexagonally packed cylinders, which allows for better charge transport than the lamellar morphology, and the fact that TFSI coordinates more weakly due to its lower charge density.  $\sigma_{NMR}$  incorporates the diffusional motions of all mobile species, even those with no net charge, whereas ois only measures the electric-field-driven movement of charged species. In other words, if there are instantaneously neutral aggregates of ions in the sample, impedance spectroscopy cannot measure them, while NMR spectroscopy can. The Haven ratio  $(H_R)$ , with the relation  $H_R = \frac{\sigma_{NMR}}{\sigma_{IS}}$  thus gives a measure of the average charged species population relative to the total number of cations and anions. For salt-based polymeric Li<sup>+</sup> electrolytes, this leads to  $H_R > 1$ . As shown **Table S4**, we measure  $H_R = 2.7$  for the LiTFSI-doped samples  $H_R = 3.6$  for the LiTfO-doped samples. These values are consistent with  $H_R$  values reported in the literature for lithium salts in PS-b-PEO electrolytes.<sup>47</sup> Additionally, the decrease in  $H_R$  we see as anion size increases (LiTfO to LiTFSI) makes sense because the larger, more diffusely charged anion discourages ion aggregation, which decreases the difference between what NMR measures and what impedance spectroscopy measures, resulting in a lower  $H_R$ . This assertion agrees with recent modeling and experiments regarding the effects of anion size on ionic mobility, which found that the cation D increases and  $H_R$  decreases as anion size increases.<sup>32,50</sup>

#### **Conclusions**

We investigated PS-b-POEM electrolytes doped with lithium salts via NMR spectroscopy and diffusometry. NMR spectroscopy enables the separate and quantitative determination of the polymer chain, Li<sup>+</sup> cation, and counter-anion dynamics. Upon measuring the cation and anion

dynamics separately from the polymer chain dynamics, we observe a large (26-49 °C) difference between the mobility temperature of the ions and the glass transition temperature of the POEM polymer phase, a difference that increases with the charge density of the anion (inversely with the anion size). We see similar trends regardless of whether the ions are moving in the PS-b-POEM block polymer or in the POEM homopolymer, so we attribute this difference to the anion size and charge density, with minimal contributions from polymer morphology or nanophase separation. Additionally, the mobility temperatures of both lithium and anions are in agreement, indicating that the two ions are experiencing similar dynamical environments. Use of the mobility temperature from NMR spectroscopy as an ion-specific probe of dynamics represents a convenient method of quantifying and understanding differences in ion dynamics and polymer chain dynamics and relative dynamical couplings.

Using <sup>1</sup>H NMR spectroscopy, we can determine the fraction of interfacial POEM in our block polymers, matching values determined via the more-established SAXS and DSC approaches. Importantly, NMR allows for a dynamics-based view of the local composition of the PS to POEM domain interface, which can be used regardless of morphology. Further investigation of the Li<sup>+</sup> and anion transport via NMR diffusometry in the block polymer and homopolymer systems reveals the morphological symmetry and tortuosity effects on diffusion along with local energetic effects via the activation energy. The diffusometry data can be applied to the Nernst-Einstein equation to estimate the conductivity within the system, and comparing these values to conductivity data from impedance spectroscopy reveals haven ratios comparable to those found in literature for PEO-based block polymer electrolytes. Using NMR spectroscopy we have characterized lithium-doped PS-b-POEM electrolytes in a complimentary manner to traditional approaches, lending additional

chemistry-specific insight into the molecular origins of ion and polymer dynamics within these electrolytes.

#### **AUTHOR INFORMATION**

# **Corresponding Authors**

Louis A. Madsen – Department of Chemistry and Macromolecules Innovation Institute, Virginia Polytechnic Institute and State University, Blacksburg, Virginia 24061, United States; orcid.org/0000-0003-4588-5183; Email: lmadsen@vt.edu

Thomas H. Epps, III – Department of Chemical & Biomolecular Engineering and Department of Materials Science & Engineering, University of Delaware, Newark, Delaware 19716, United States; orcid.org/0000-0002-2513-0966; Email: thepps@udel.edu

## Authors

Nicholas F. Pietra – Department of Chemistry and Macromolecules Innovation Institute, Virginia Polytechnic Institute and State University, Blacksburg, Virginia 24061, United States; https://orcid.org/0000-0003-3250-728X

Andrew G. Korovich – Department of Chemistry and Macromolecules Innovation Institute, Virginia Polytechnic Institute and State University, Blacksburg, Virginia 24061, United States; https://orcid.org/0000-0003-3736-1523

Priyanka M. Ketkar – Department of Chemical & Biomolecular Engineering, University of Delaware, Newark, Delaware 19716, United States; https://orcid.org/0000-0001-8891-4808

### **Author Contributions**

The manuscript was written through contributions of all authors. N.F.P., A.G.K., and P.M.K. contributed equally to this work. All authors have given approval to the final version of the manuscript.

#### **Notes**

The authors declare no competing financial interest.

#### SUPPORTING INFORMATION

Detailed information behind determination of mobility temperatures from <sup>7</sup>Li, <sup>19</sup>F, and <sup>1</sup>H spectra; further explanation behind method to determine interfacial POEM fraction from DSC, SAXS, and <sup>1</sup>H NMR spectra applied to lamellar and cylindrical morphologies; diffusometry data; and tortuosity and conductivity determinations.

## ACKNOWLEDGMENT

N.F.P., A.G.K., and L.A.M. thank the National Science Foundation (DMR Polymers – 1810194) for financial support for the NMR characterization of solid electrolyte samples and for the undertaking of this project. P.M.K. and T.H.E. thank a Department of Energy grant (DOE BES; DE-SC0014458) for financial support during polymer synthesis, sample preparation, and sample characterization. The authors thank Dr. Melody A. Morris for the synthesis of the PS and POEM homopolymers. Certain commercial equipment, instruments, materials, suppliers, or software are identified in this paper to facilitate the understanding and interpretation of data. Such identifications do not imply recommendation or endorsement by DOE or NSF, nor do they imply that the materials or equipment identified are necessarily the best available for the purpose.

#### References

- (1) Arya, A.; Sharma, A. L. A glimpse on all-solid-state Li-ion battery (ASSLIB) performance based on novel solid polymer electrolytes: a topical review. *Journal of Materials Science* **2020**, 55 (15), 6242-6304. DOI: 10.1007/s10853-020-04434-8.
- (2) Chen, Y.; Kang, Y.; Zhao, Y.; Wang, L.; Liu, K.; Li, Y.; Liang, Z.; He, X.; Li, X.; Tavajohi, N.; et al. A review of lithium-ion battery safety concerns: the issue, strategies, and testing standards. *Journal of Energy Chemistry* **2021**, *59*, 83-99. DOI: 10.1016/j.jechem.2020.10.017.
- (3) Fenton, D. E.; Parker, J. M.; Wright, P. V. Complexes of alkali metal ions with poly(ethylene oxide). *Polymer* **1973**, *14* (11), 589. DOI: <a href="https://doi.org/10.1016/0032-3861(73)90146-8">https://doi.org/10.1016/0032-3861(73)90146-8</a>.
- (4) Xue, Z.; He, D.; Xie, X. Poly(ethylene oxide)-based electrolytes for lithium-ion batteries. *Journal of Materials Chemistry A* **2015**, *3* (38), 19218-19253. DOI: 10.1039/c5ta03471j.
- (5) Rosenwinkel, M. P.; Schönhoff, M. Lithium Transference Numbers in PEO/LiTFSA Electrolytes Determined by Electrophoretic NMR. *Journal of The Electrochemical Society* **2019**, *166* (10), A1977-A1983. DOI: 10.1149/2.0831910jes.
- (6) Nie, K.; Wang, X.; Qiu, J.; Wang, Y.; Yang, Q.; Xu, J.; Yu, X.; Li, H.; Huang, X.; Chen, L. Increasing Poly(ethylene oxide) Stability to 4.5 V by Surface Coating of the Cathode. *ACS Energy Letters* **2020**, *5* (3), 826-832. DOI: 10.1021/acsenergylett.9b02739.
- (7) Gorecki, W.; Jeannin, M.; Belorizky, E.; Roux, C.; Armand, M. Physical properties of solid polymer electrolyte PEO(LiTFSI) complexes. *Journal of Physics: Condensed Matter* **1995**, 7 (34), 6823. DOI: 10.1088/0953-8984/7/34/007.
- (8) Mirsakiyeva, A.; Ebadi, M.; Araujo, C. M.; Brandell, D.; Broqvist, P.; Kullgren, J. Initial Steps in PEO Decomposition on a Li Metal Electrode. *The Journal of Physical Chemistry C* **2019**, *123* (37), 22851-22857. DOI: 10.1021/acs.jpcc.9b07712.
- (9) Yuan, R.; Teran, A. A.; Gurevitch, I.; Mullin, S. A.; Wanakule, N. S.; Balsara, N. P. Ionic conductivity of low molecular weight block copolymer electrolytes. *Macromolecules* **2013**, *46* (3), 914-921. DOI: 10.1021/ma3024552.
- (10) Hallinan, D. T.; Balsara, N. P. Polymer Electrolytes. *Annual Review of Materials Research* **2013**, *43* (1), 503-525. DOI: 10.1146/annurev-matsci-071312-121705.
- (11) Chintapalli, M.; Le, T. N. P.; Venkatesan, N. R.; Mackay, N. G.; Rojas, A. A.; Thelen, J. L.; Chen, X. C.; Devaux, D.; Balsara, N. P. Structure and ionic conductivity of polystyrene-*block*-poly(ethylene oxide) electrolytes in the high salt concentration limit. *Macromolecules* **2016**, 49 (5), 1770-1780. DOI: 10.1021/acs.macromol.5b02620.
- (12) Gomez, E. D.; Panday, A.; Feng, E. H.; Chen, V.; Stone, G. M.; Minor, A. M.; Kisielowski, C.; Downing, K. H.; Borodin, O.; Smith, G. D.; et al. Effect of ion distribution on conductivity of block copolymer electrolytes. *Nano Letters* **2009**, *9* (3), 1212-1216.
- (13) Loo, W. S.; Balsara, N. P. Organizing thermodynamic data obtained from multicomponent polymer electrolytes: salt-containing polymer blends and block copolymers. *Journal of Polymer Science Part B-Polymer Physics* **2019**, *57* (18), 1177-1187. DOI: 10.1002/polb.24800.
- (14) Loo, W. S.; Galluzzo, M. D.; Li, X.; Maslyn, J. A.; Oh, H. J.; Mongcopa, K. I.; Zhu, C.; Wang, A. A.; Wang, X.; Garetz, B. A.; et al. Phase Behavior of Mixtures of Block Copolymers and a Lithium Salt. *J Phys Chem B* **2018**, *122* (33), 8065-8074. DOI: 10.1021/acs.jpcb.8b04189.
- (15) Bennington, P.; Deng, C. T.; Sharon, D.; Webb, M. A.; de Pablo, J. J.; Nealey, P. F.; Patel, S. N. Role of solvation site segmental dynamics on ion transport in ethylene-oxide based side-

- chain polymer electrolytes. *Journal of Materials Chemistry A* **2021**, *9* (15), 9937-9951. DOI: 10.1039/d1ta00899d.
- (16) Deng, C. T.; Webb, M. A.; Bennington, P.; Sharon, D.; Nealey, P. F.; Patel, S. N.; de Pablo, J. J. Role of molecular architecture on ion transport in ethylene oxide-based polymer electrolytes. *Macromolecules* **2021**, *54* (5), 2266-2276. DOI: 10.1021/acs.macromol.0c02424.
- (17) Ketkar, P. M.; Pietra, N. F.; Korovich, A.; Madsen, L. A.; Epps III, T. H. Role of intra-domain heterogeneity on ion and polymer dynamics in block polymer electrolytes: An approach for spatially resolving dynamics and ion transport. *Macromolecules* **2023**, *To be published*.
- (18) Teran, A. A.; Balsara, N. P. Thermodynamics of Block Copolymers with and without Salt. *The Journal of Physical Chemistry B* **2014**, *118* (1), 4-17.
- (19) Young, W.-S.; Epps III, T. H. Salt doping in PEO-containing block copolymers: counterion and concentration effects. *Macromolecules* **2009**, *42* (7), 2672-2678.
- (20) Brown, J. R.; Seo, Y.; Hall, L. M. Ion Correlation Effects in Salt-Doped Block Copolymers. *Phys Rev Lett* **2018**, *120* (12), 127801. DOI: 10.1103/PhysRevLett.120.127801.
- (21) Sing, C. E.; Zwanikken, J. W.; Olvera de la Cruz, M. Electrostatic control of block copolymer morphology. *Nat Mater* **2014**, *13* (7), 694-698. DOI: 10.1038/nmat4001.
- (22) Levitt, M. H. Spin dynamics: basics of nuclear magnetic resonance; John Wiley & Sons, 2013.
- (23) Bostwick, J. E.; Zanelotti, C. J.; Yu, D.; Pietra, N. F.; Williams, T. A.; Madsen, L. A.; Colby, R. H. Ionic interactions control the modulus and mechanical properties of molecular ionic composite electrolytes. *Journal of Materials Chemistry C* **2022**, *10* (3), 947-957. DOI: 10.1039/d1tc04119c.
- (24) Yu, D.; Pan, X.; Bostwick, J. E.; Zanelotti, C. J.; Mu, L.; Colby, R. H.; Lin, F.; Madsen, L. A. Room Temperature to 150° C Lithium Metal Batteries Enabled by a Rigid Molecular Ionic Composite Electrolyte. *Advanced Energy Materials* **2021**, *11* (12), 2003559.
- (25) Kidd, B. E.; Forbey, S. J.; Steuber, F. W.; Moore, R. B.; Madsen, L. A. Multiscale Lithium and Counterion Transport in an Electrospun Polymer-Gel Electrolyte. *Macromolecules* **2015**, 48 (13), 4481-4490. DOI: 10.1021/acs.macromol.5b00573.
- (26) Zhang, R.; Troya, D.; Madsen, L. A. Prolonged Association between Water Molecules under Hydrophobic Nanoconfinement. *The Journal of Physical Chemistry B* **2021**, *125* (50), 13767-13777. DOI: 10.1021/acs.jpcb.1c06810.
- (27) Lingwood, M. D.; Zhang, Z. Y.; Kidd, B. E.; McCreary, K. B.; Hou, J. B.; Madsen, L. A. Unraveling the local energetics of transport in a polymer ion conductor. *Chemical Communications* **2013**, *49* (39), 4283-4285. DOI: 10.1039/c2cc37173a.
- (28) Ketkar, P. M.; Shen, K.-H.; Fan, M.; Hall, L. M.; Epps, T. H., III. Quantifying the effects of monomer segment distributions on ion transport in tapered block polymer electrolytes. *Macromolecules* **2021**, *54* (16), 7590-7602. DOI: 10.1021/acs.macromol.1c00941.
- (29) Morris, M. A.; Sung, S. H.; Ketkar, P. M.; Dura, J. A.; Nieuwendaal, R. C.; Epps, T. H., III. Enhanced conductivity *via* homopolymer-rich pathways in block polymer-blended electrolytes. *Macromolecules* **2019**, *52* (24), 9682-9692. DOI: 10.1021/acs.macromol.9b01879.
- (30) Stejskal, E. O.; Tanner, J. E. Spin Diffusion Measurements: Spin Echoes in the Presence of a Time-Dependent Field Gradient. *The Journal of Chemical Physics* **1965**, *42* (1), 288-292. DOI: 10.1063/1.1695690.
- (31) Tanner, J. E. Use of the Stimulated Echo in NMR Diffusion Studies. *The Journal of Chemical Physics* **1970**, *52* (5), 2523-2526. DOI: 10.1063/1.1673336.

- (32) Shen, K.-H.; Hall, L. M. Effects of Ion Size and Dielectric Constant on Ion Transport and Transference Number in Polymer Electrolytes. *Macromolecules* **2020**, *53* (22), 10086-10096. DOI: 10.1021/acs.macromol.0c02161.
- (33) Huynh, T. V.; Messinger, R. J.; Sarou-Kanian, V.; Fayon, F.; Bouchet, R.; Deschamps, M. Restricted lithium ion dynamics in PEO-based block copolymer electrolytes measured by high-field nuclear magnetic resonance relaxation. *J Chem Phys* **2017**, *147* (13), 134902. DOI: 10.1063/1.4993614.
- (34) Kuan, W.-F.; Reed, E. H.; Nguyen, N. A.; Mackay, M. E.; Epps, T. H. Using tapered interfaces to manipulate nanoscale morphologies in ion-doped block polymers. *MRS Communications* **2015**, *5* (2), 251-256. DOI: 10.1557/mrc.2015.19.
- (35) Liu, J. C.; Pickett, P. D.; Park, B.; Upadhyay, S. P.; Orski, S. V.; Schaefer, J. L. Non-solvating, side-chain polymer electrolytes as lithium single-ion conductors: synthesis and ion transport characterization. *Polymer Chemistry* **2020**, *11* (2), 461-471. DOI: 10.1039/c9py01035a.
- (36) Morèse-Séguéla, B.; St-Jacques, M.; Renaud, J. M.; Prud'homme, J. Microphase separation in low molecular weight styrene-isoprene diblock copolymers studied by DSC and <sup>13</sup>C NMR. *Macromolecules* **1980**, *13*, 100-106.
- (37) Burns, A. B.; Christie, D.; Mulhearn, W. D.; Register, R. A. Estimating the segregation strength of microphase-separated diblock copolymers from the interfacial width. *Journal of Polymer Science Part B: Polymer Physics* **2019**, *57* (14), 932-940. DOI: 10.1002/polb.24848.
- (38) Sax, J.; Ottino, J. Modeling of transport of small molecules in polymer blends: Application of effective medium theory. *Polymer Engineering & Science* **1983**, *23* (3), 165-176.
- (39) Hallinan, D. T.; Villaluenga, I.; Balsara, N. P. Polymer and composite electrolytes. *MRS Bulletin* **2018**, *43* (10), 759-767. DOI: 10.1557/mrs.2018.212.
- (40) Kidd, B. E.; Lingwood, M. D.; Lee, M.; Gibson, H. W.; Madsen, L. A. Cation and anion transport in a dicationic imidazolium-based plastic crystal ion conductor. *J Phys Chem B* **2014**, *118* (8), 2176-2185. DOI: 10.1021/jp4084629.
- (41) Thieu, L. M.; Zhu, L.; Korovich, A. G.; Hickner, M. A.; Madsen, L. A. Multiscale tortuous diffusion in anion and cation exchange membranes. *Macromolecules* **2018**, *52* (1), 24-35.
- (42) Chang, K.; Korovich, A.; Xue, T.; Morris, W. A.; Madsen, L. A.; Geise, G. M. Influence of rubbery versus glassy backbone dynamics on multiscale transport in polymer membranes. *Macromolecules* **2018**, *51* (22), 9222-9233.
- (43) Korovich, A. G.; Chang, K.; Geise, G. M.; Madsen, L. A. Local Water Transport in Rubbery versus Glassy Separation Membranes and Analogous Solutions. *Macromolecules* **2021**, *54* (23), 11187-11197. DOI: 10.1021/acs.macromol.1c01746.
- (44) Zhang, R.; Chen, Y.; Troya, D.; Madsen, L. A. Relating Geometric Nanoconfinement and Local Molecular Environment to Diffusion in Ionic Polymer Membranes. *Macromolecules* **2020**, *53* (9), 3296-3305. DOI: 10.1021/acs.macromol.9b02755.
- (45) Hou, J.; Li, J.; Mountz, D.; Hull, M.; Madsen, L. A. Correlating morphology, proton conductivity, and water transport in polyelectrolyte-fluoropolymer blend membranes. *Journal of Membrane Science* **2013**, *448*, 292-299. DOI: 10.1016/j.memsci.2013.08.019.
- (46) Shen, K. H.; Brown, J. R.; Hall, L. M. Diffusion in Lamellae, Cylinders, and Double Gyroid Block Copolymer Nanostructures. *ACS Macro Lett* **2018**, 7 (9), 1092-1098. DOI: 10.1021/acsmacrolett.8b00506.
- (47) Timachova, K.; Villaluenga, I.; Cirrincione, L.; Gobet, M.; Bhattacharya, R.; Jiang, X.; Newman, J.; Madsen, L. A.; Greenbaum, S. G.; Balsara, N. P. Anisotropic Ion Diffusion and

- Electrochemically Driven Transport in Nanostructured Block Copolymer Electrolytes. *J Phys Chem B* **2018**, *122* (4), 1537-1544. DOI: 10.1021/acs.jpcb.7b11371.
- (48) Bostwick, J. E.; Zanelotti, C. J.; Iacob, C.; Korovich, A. G.; Madsen, L. A.; Colby, R. H. Ion Transport and Mechanical Properties of Non-Crystallizable Molecular Ionic Composite Electrolytes. *Macromolecules* **2020**, *53* (4), 1405-1414. DOI: 10.1021/acs.macromol.9b02125.
- (49) France-Lanord, A.; Grossman, J. C. Correlations from Ion Pairing and the Nernst-Einstein Equation. *Phys Rev Lett* **2019**, *122* (13), 136001. DOI: 10.1103/PhysRevLett.122.136001.
- (50) Mei, W.; Yu, D.; George, C.; Madsen, L. A.; Hickey, R. J.; Colby, R. H. Anion chemical composition of poly (ethylene oxide)-based sulfonylimide and sulfonate lithium ionomers controls ion aggregation and conduction. *Journal of Materials Chemistry C* **2022**, *10* (39), 14569-14579.